4 Sample Preparation and Measurement Strategies

> [. . .] une œuvre d'homme n'est rien d'autre que ce long cheminement pour retrouver par les détours de l'art les deux ou trois images simples et grandes sur lesquelles le cœur, une première fois, s'est ouvert.
>
> *(Albert Camus, L'envers et l'endroit)*

4.1 Introduction

Science lives by the reproducibility and falsifiability of its results. Even if such accounts rarely make for exciting reading, it is therefore of vital importance to provide as much data on the experimental procedure as is necessary to reproduce experiments independently, at least as far as this is possible within the context of publication.

The motivation for this chapter is twofold: First, to provide the background information that—it is to be hoped—puts the reader in the position to fully assess and reproduce the results presented here. To this end I shall report on the details of the experimental procedure where relevant and discuss several technologies with a focus on their use in the present work. Second, to collect all technical information in a convenient place to which one can refer back if necessary. In this way, I can omit these particulars from the discussion of physical phenomena, while still ensuring that they are readily available if needed.

In Sec. 4.2 I shall describe the technologies used for producing samples from double heterostructures (DHETs) that are suitable for magnetotransport measurements and for creating modulations on them. In this context, Secs. 4.2.1, 4.2.2, 4.2.3, and 4.2.4 focus on lithographic

techniques, while 4.2.5 and 4.2.6 discuss methods for transferring patterns created in a surface layer into the semiconductor by etching. Sec. 4.3 explains the equipment and methodology employed in performing magnetotransport experiments on these samples.

4.2 Fabrication Techniques

4.2.1 Optical Lithography

Optical lithography is a standard technique in semiconductor processing. One can distinguish positive processes, in which the exposed area is removed during development, and negative ones, in which exposed areas are retained while the rest of the photoactive film is removed [1]. Positive optical resist is generally based on the 'novolak' resin,

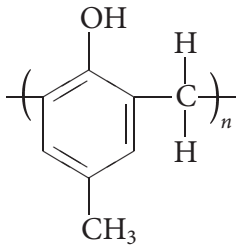

, (4.1)

which is mixed with a strong dissolution inhibitor derived from diazonaphthoquinone (DNQ). Exposure to ultraviolet (UV) radiation changes DNQ into a ketene, which takes up water to form a carboxylic acid:

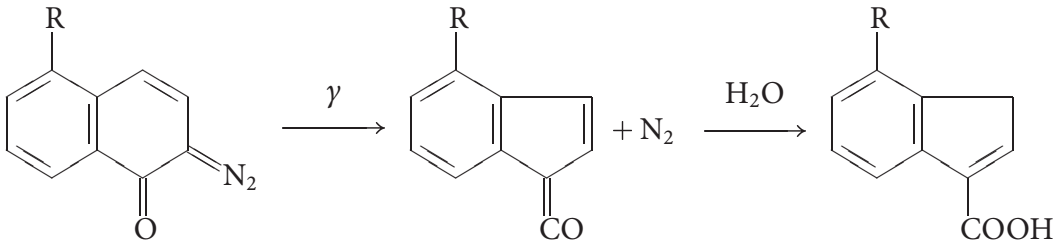

(4.2)

The carboxylic acid acts as a weak dissolution promoter [2].

In this work, SHIPLEY MICROPOSIT S1813 positive resist was used together with SHIPLEY MF319 developer. The resist was spun on at 5,000 rpm for 50 s and then baked at 100 °C for

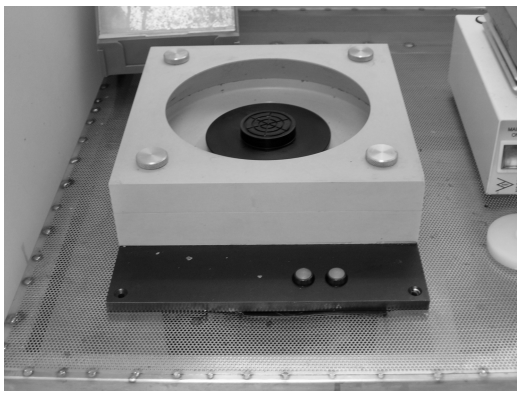

(a) Spinner

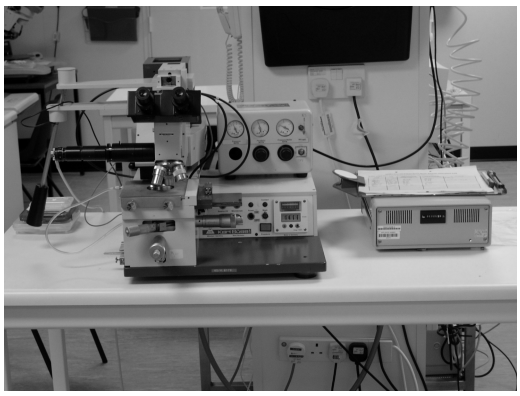

(b) Karl Süss MJB3 mask aligner

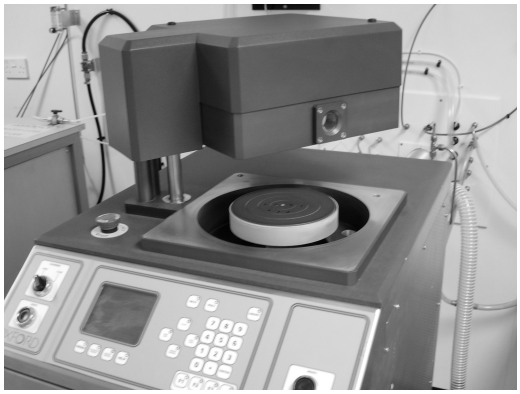

(c) Oxford Instruments RIE80+ reactive ion etcher

Figure 4.1: Clean room equipment

5 min by means of the conventional spinner seen in Fig. 4.1(a). Using a scanning electron microscope (SEM) to assess the transfer of strip patterns after development for 60 s, an optimal exposure time of 11 ± 1 s was determined for the Karl Süss MJB3 mask aligner of Fig. 4.1(b) with a new mercury vapour lamp.

The complete optical lithography process is explained in Fig. 4.2 for the creation of a Hall bar-shaped mesa on a DHET. First, the photoresist was spun on the surface and baked to drive out the solvent and prevent sticking of the sample to the mask. The desired pattern was then exposed with a mask aligner and the exposed photoresist removed during development. In the next step, the surface was etched using one of the recipes described in Sec. 4.2.5 or 4.2.6. Usually a wet chemical etch was employed, as the inhomogeneous etch rate that can be

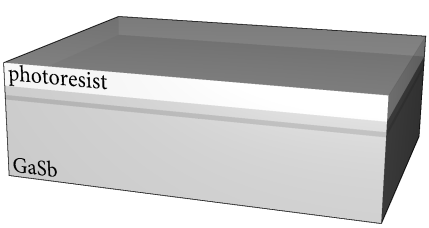

(a) Spinning on photoresist

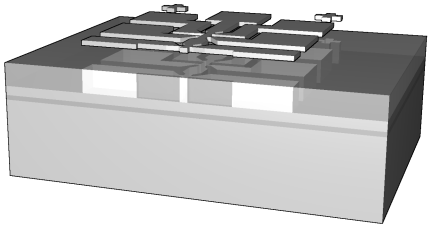

(b) Exposure of resist with contact mask

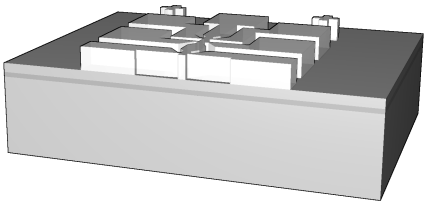

(c) Development of resist

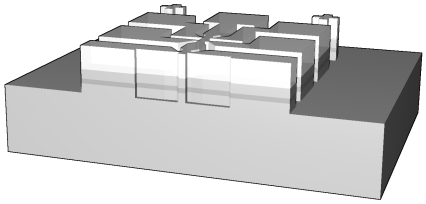

(d) RIE or wet etch of semiconductor

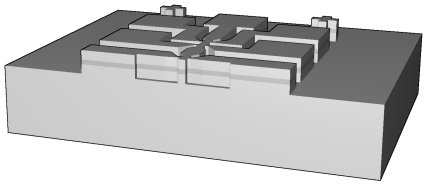

(e) Removal of photoresist in acetone or stripper

Figure 4.2: Optical lithography. In this example, a Hall bar pattern including contact pads is created using positive photoresist. The vertical scale is exaggerated.

achieved with a plasma etch was not vital for comparatively shallow etches at the resolution of the optical process. Finally, the remaining photoresist mask could be removed in acetone or resist stripper.

4.2.2 Electron Beam Lithography

Optical lithography is restricted by diffraction and has a finite depth of field. The practical resolution limit with deep UV light is approximately 0·15 µm, while 0·01 µm can be realized with hard X-rays [1]. Contact exposure with near UV light, which is useful in the laboratory for prototyping, achieves in practice a resolution of 0·8 to 1·0 µm. Electron beam lithography (EBL) is an alternative to optical lithography that uses electrons instead of photons and does not suffer from these effects. The wave length of the electrons is much smaller than the practical resolution limit given by the chemical properties of the sensitive layer and the quality of the beam focusing column, which is used instead of a mask to define the pattern.

As resist, EBL uses a polymer such as poly-(methyl-methacrylate) (PMMA),

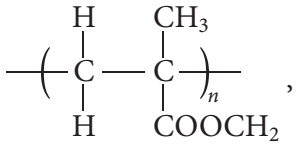

(4.3)

the chains of which can be broken by electron bombardment. The resulting oligomers become soluble and are removed during development, so that the polymer acts as a positive resist [2]. For very high doses, the opposite effect can be observed: exposed areas become insoluble even in solvents that readily attack the unmodified polymer. This effect is thought to be due to cross-linking and offers the possibility of creating negative patterns [3].

PMMA offers the highest available resolution—less than 10 nm is possible for isolated features [4]—but has a poor resistance to many etch plasmas, which erode the mask quickly by sputtering. This is particularly problematic for reactive ion etching (RIE) of III–V semiconductors, as the semiconductor etch rate is low. Several alternative chemistries have been

proposed to address this problem, one of the most successful ones being Nippon Zeon zep, which is based on poly-(methyl-chloroacrylate-co-α-methylstyrene):

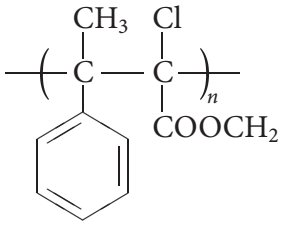

(4.4)

Similar to pmma, exposure of zep causes chain scission and the chemical acts as a positive-tone resist.

ebl is affected by proximity effects caused by secondary electrons. Randomly scattered electrons induce a limited exposure of the resist film immediately around the nominally exposed areas. Although overexposure can be avoided by calculating the magnitude of the effect and correcting the dose accordingly, dense patterns suffer from a significant reduction in the contrast between exposed and unexposed areas and the resolution is worse than for isolated lines.

Most of the electron beam work was done in the Cavendish Laboratory in Cambridge with the help of Geb Jones, because the facilities available in Oxford would only allow for a limited resolution. We used both pmma and zep resist layers, each spun on the sample to give a film thickness of approximately 300 nm. pmma was baked at 180 °C for 1 h before exposure and developed for 10 s in a mixture of 583 parts methyl-ethyl-ketone, 1,617 parts ethanol, 30 parts 2-ethoxyethanol, 70 parts methanol, 1 part methyl-isobutyl-ketone (mibk), and 3 parts isopropanol (ipa). zep films were baked at 180 °C for 5 min. They were developed for 1 min in amyl-acetate followed by a 10 s rinse in a developer consisting of 9 parts mibk and 1 part ipa. Optimal exposure varied as a result of the proximity effect, with typical values around 90 µC/cm^2 for pmma and 300 µC/cm^2 for zep.

The use of zep to create more resistant etch masks for the rie of GaSb and InAs was only partly successful. Untreated zep films were etched with an etch rate of 20 to 30 nm/min in an argon-free hydrogen–methane plasma, comparable to etch rate of pmma. For some

samples, this could be improved by thermal treatment at 145 °C for 2 h, yielding etch rates of 3 to 10 nm/min. The heat treatment appeared to be effective only if performed within a few days of development, and the results were inconsistent. The underlying chemical mechanism is not understood, and both the high etch rates observed initially and the thermal hardening may conceivably be connected to contaminants introduced during processing.

Another approach that can be employed to compensate for the poor etch resistance of PMMA is the use of an intermediate mask layer. SiO_2 has a negligible etch rate in hydrogen–methane plasmas, but can be etched readily using a freon-based recipe [5]. Fig. 4.3 illustrates the creation of antidot arrays by means of this technique: After a 40 nm thick silicon dioxide layer was evaporated on the sample and the resist was spun on, the dots were exposed in an electron beam writer. Development created a resist mask, which was used to transfer the pattern to the silicon dioxide layer using a freon-based etch plasma. The patterned oxide film then served as a mask for etching the InAs–GaSb DHET; during this process, the original PMMA mask was typically removed completely. Finally, the SiO_2 could be removed in hydrofluoric acid.

4.2.3 Direct Surface Modification by Local Anodic Oxidation

LAO can be used to oxidize a GaSb surface directly; the process has been described in detail in Chapter 3. The method makes it possible to fabricate oxide dot arrays covering a limited area such as the surface of a Hall bar. Oxide dots may then be dissolved in water or hydrochloric acid, leaving holes at most 20 nm deep. Fig. 4.4 illustrates the procedure.

Since features created by LAO are generally not visible in an optical microscope [6], alignment marks or mesas must be defined on the surface before the atomic force microscope (AFM) patterning—alignment would be impossible the other way around. As a result of the standard lithographical process described in Sec. 4.2.1, organic residue will be present on the surface, which can stick to the AFM probe and interfere with anodization (see Fig. 4.5). Such residue can routinely be removed in a RIE setup with an oxygen plasma, a process commonly

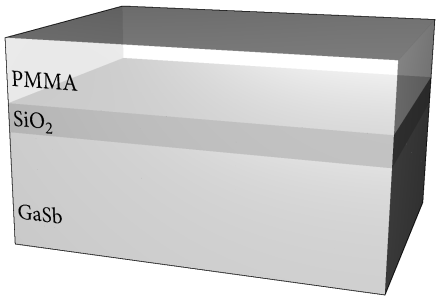

(a) Evaporation of silica and resist coating

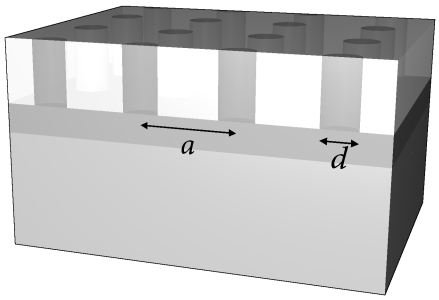

(b) Exposure of resist with electron beam

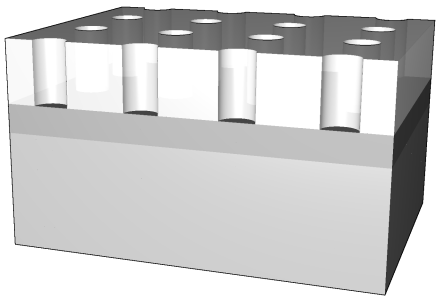

(c) Development of resist

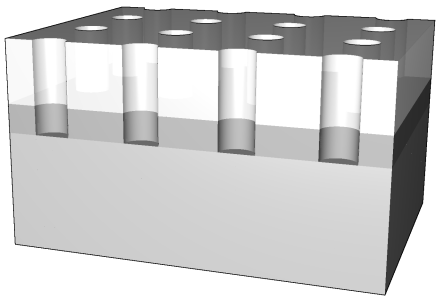

(d) RIE of silica

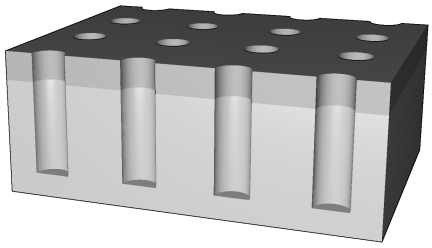

(e) RIE of GaSb

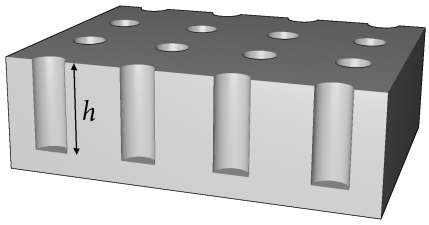

(f) Chemical removal of silica in HF

Figure 4.3: Electron beam lithography. In this example, holes with diameter d, lattice constant a, and depth h are created. An intermediate silica mask is used.

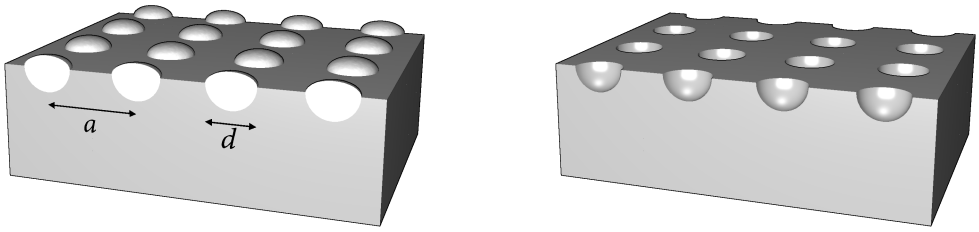

(a) Local anodization with the AFM (b) Chemical removal of oxide dots

Figure 4.4: Direct surface modification with the AFM. In this example, holes with diameter d and lattice constant a are created by LAO.

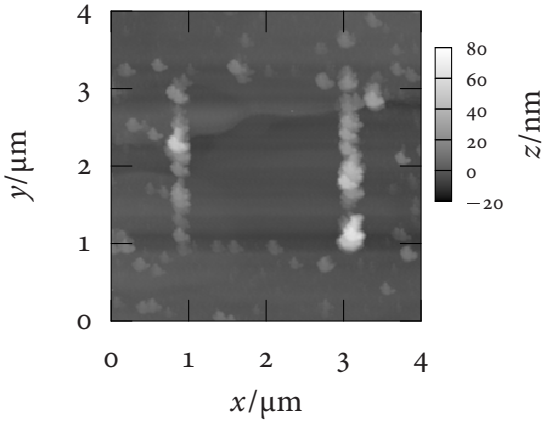

Figure 4.5: AFM micrograph showing organic residue after optical lithography. The central square has been swept clear by scanning in contact mode. Repeating features representative of tip geometry are clearly visible; they are believed to be caused by pick-up of contaminants.

referred to as 'ashing' [7,8]. As an oxygen plasma was not available in the standard configuration of the RIE equipment available to me, an argon plasma was substituted in most cases, which is sufficient to remove thin organic layers by sputtering.

4.2.4 Creation of Aluminium Etch Masks by Local Anodic Oxidation

Direct modification of semiconductor surfaces by oxidation with an AFM is limited by the finite oxide thickness that can be achieved with this method. It is therefore desirable to have the option of transferring the lithographic patterns into the sample using an etch technique such as RIE that is capable of producing deeper features with a larger aspect ratio. This is possible if LAO can be used to create a suitable etch mask.

Silica withstands many useful RIE chemistries, including the hydrogen and methane based recipes usually employed to etch III–V semiconductors. The oxide formed by local anodization of silicon can therefore be used as an etch mask [9,10]. A similar approach using the oxidation of thin aluminium layers has been proposed by Anja Boisen *et al.* [11,12]. Both aluminium and aluminium oxide can be used as effective etch masks for RIE of both silicon and III–V semiconductors, and it is possible to selectively remove either the unoxidized aluminium or the oxide features in a wet etch solution without compromising the lithographic resolution. Such a metal layer may therefore be used as either a positive or negative resist. Al can be removed in 85 % phosphoric acid at room temperature, whereas selective removal of Al_2O_3 can be accomplished in a mixture of phosphoric acid, deionized water, and chromiumtrioxide at approximately 50 °C. If necessary, the aluminium or aluminium oxide may be removed in hydrofluoric acid.

The possibility of a positive process makes the method attractive for the creation of antidot patterns. Exposure of the entire area between the dots takes much longer than drawing individual dots. The risk of tip failure would be increased; moreover, protecting the contact leads would require an additional process step. I have therefore adapted the creation of aluminium masks to GaSb surfaces. Sec. 3.7 describes the LAO of thin aluminium layers and

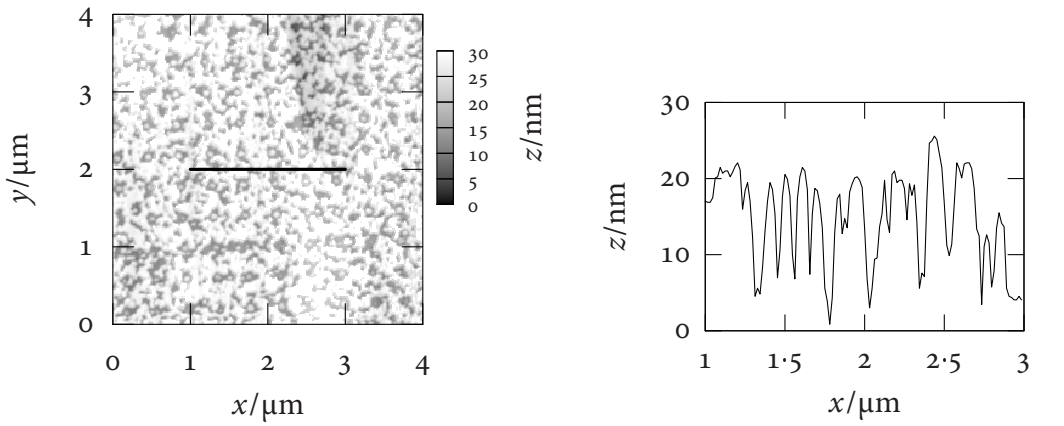

(a) AFM micrograph of eroded Al layer (b) Height profile at the line indicated in (a)

Figure 4.6: Erosion of aluminium layers on GaSb in oxide stripper. Remnants of an antidot pattern are discernible in (a).

indicates that up to 20 nm thick films can be oxidized completely with a minimal feature size of approximately 130 nm. For mask applications, aluminium layers with a nominal thickness of 10 nm to 15 nm were chosen, and it was verified that such layers would withstand a typical RIE recipe for etching GaSb and InAs (recipe B from Sec. 4.2.6) for long enough to etch roughly 200 nm of GaSb.

For the selective removal of anodized aluminium, an etchant consisting of 3·5 ml H_3PO_4 (85 %), 100 ml DI-H_2O, and 2·0 g CrO_3 at 60 °C was used [13]. Initial attempts at selective removal of oxide dots in aluminium layers evaporated directly on GaSb epilayers were unsuccessful: the aluminium layer was quickly attacked in the oxide stripper before the oxide could be removed completely. Within 1 to 4 min, holes were opened in the aluminium layer down to the underlying GaSb, leading to a characteristic erosion pattern illustrated in Fig. 4.6. By comparing the behaviour of oxide layers on GaSb and Si processed under identical conditions, it was established that this effect is specific to aluminium films on GaSb and not caused by any other effect such as external contaminants.

The chemical mechanism of this erosion caused by the presence of the GaSb surface is not fully understood. One possible explanation is the presence of Ga or Sb in the aluminium

layer because of interdiffusion. The problem could be avoided by introducing a high-quality SiO_2 spacer layer created by ion-beam assisted evaporation between the GaSb surface and the Al layer; a layer thickness of 40 nm was chosen. As explained in Sec. 4.2.6, silicon dioxide can be etched in a freon-based plasma and such an additional etch step can be added before the hydrogen–methane etch without having to remove the sample from the reaction chamber. As with direct manipulation of the surface, it is necessary to define either alignment marks or entire Hall bars by optical lithography prior to LAO, since it is not possible to align optical masks to features created by AFM patterning. This may be done either by defining and etching devices before the SiO_2 and Al layers are applied, or by patterning the Al layer and using it as a mask for the RIE of both the contact leads and the nanoscopic patterns. Both methods have drawbacks which caused the failure of a number of devices, leading to a reduced yield. On predefined mesas, the silica covering of sidewalls was imperfect, and the same erosion pattern as described above usually appeared in a strip of oxide several micron wide on both sides of the step. Since small Hall bars (typically 5 or 10 µm wide) were required to allow complete patterning in the AFM, such a defect could completely affect the active area of a device. If the Al layer was to be patterned by optical lithography, cracking of the underlying silica film sometimes occurred during development of the optical resist; such cracks often caused similar failures as edges and acted as starting points for peeling of the evaporated mask layers in the RIE.

The full fabrication process is illustrated in Fig 4.7: First, SiO_2 and Al layers were created by evaporation, possibly patterning the Al layer using optical lithography. The Al film was then locally oxidized down to the underlying SiO_2 with an AFM and the oxide was removed in the oxide stripper, leaving holes in the aluminium layer. The aluminium layer served as a mask for the plasma etching of the silicon dioxide and the InAs–GaSb heterostructure. Finally, both the Al and the SiO_2 films were removed in hydrofluoric acid, exposing the patterned semiconductor. Fig. 4.8 shows a test pattern before and after the critical oxide removal step, corresponding to Fig. 4.7(b) and Fig. 4.7(c), respectively.

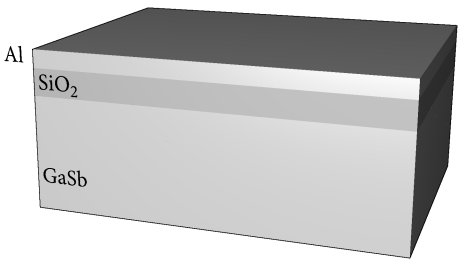

(a) Evaporation of silica and Al

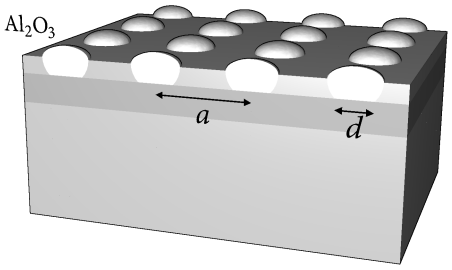

(b) Local anodization with the AFM

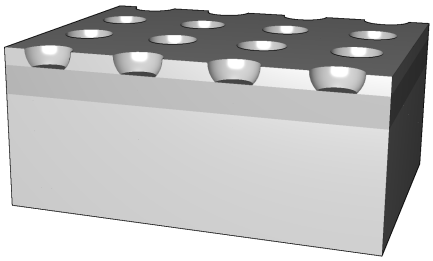

(c) Chemical removal of anodized Al

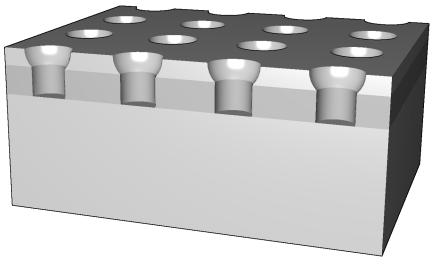

(d) RIE of silica

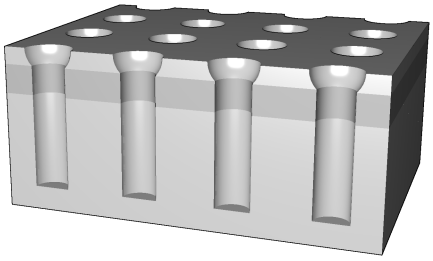

(e) RIE of GaSb

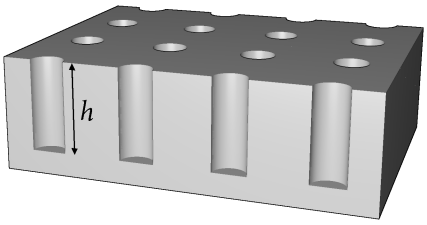

(f) Chemical removal of the mask in HF

Figure 4.7: Pattern transfer using an AFM-created RIE mask. In this example, holes with diameter d, lattice constant a, and depth h are created in GaSb, which is protected from the selective alumina etch by a silica layer.

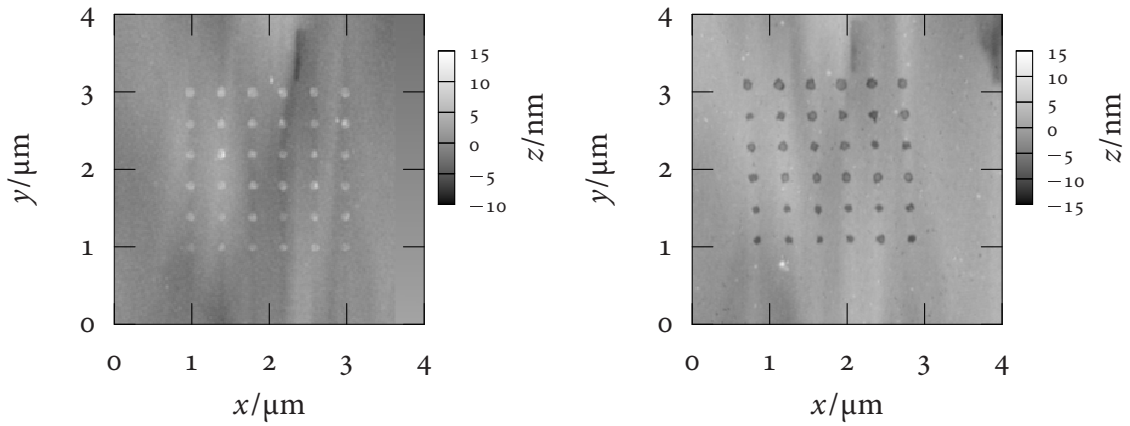

(a) Before removal of oxide

(b) After removal of oxide

Figure 4.8: AFM micrographs of an aluminium etch mask created by LAO

4.2.5 Wet Chemical Etching

I used two different wet etch solutions for shaping InAs–GaSb DHETs; wet etching served predominantly to create mesa structures, such as Hall bars, that pattern the InAs quantum well and enable transport measurements in a well-defined geometry.

BUGLASS *et al.* [14] have proposed an etchant that is suitable for III–V semiconductors containing antimony, as it contains $(C_4H_4O_6)^{2-}$ tartrate ions that react with Sb to form a soluble complex, thereby preventing the formation of a protective layer of antimony oxide. The actual etchant is an aqueous solution containing 0·1 mol $(NH_4)_2$ $(C_4H_4O_6)$, 1·0 mol HCl, and 0·5 mol H_2O_2 per litre. During the etching of (100)-GaSb, gas bubbles develop and the surface is roughened noticeably. The etchant ages quickly and the etch rate varies accordingly. In the interest of reproducibility, the solution was allowed to stabilize for 20 min, whereafter an isotropic etch rate of approximately 100 nm/min was determined for GaSb by measuring etch steps using an AFM. This agrees with the values found by CHRISTOPHER BUMBY [15], who reports an initial rate of 200 nm/min, decreasing significantly within 30 min. The etch rate on InAs is much less, and a surface layer is eventually formed that prevents further erosion [15]; for the thin (30 nm) InAs quantum wells present in the DHETs of interest here, this effect did not pose a problem.

An alternative system, originally proposed by Adachi *et al.* [16] in a slightly different form, uses the dichromate ion, $(Cr_2O_7)^{2-}$, as an oxidizing agent. It etches most III–V semiconductors isotropically and with little roughening. The etchant was prepared as an aqueous solution containing 0·0367 mol $K_2Cr_2O_7$ (potassium dichromate), 3·97 mol HBr (hydrobromic acid), and 5·83 mol CH_3COOH (acetic acid) per litre; the comparatively low dichromate concentration originated from the use of a commercially available prepared solution. With this recipe, etch rates of approximately 2,000 nm/min for (100)-GaSb and 2,800 nm/min for (111)-InSb were observed for shallow ($\gtrsim 1\,\mu m$) etches. This does not contradict the the lower values around 200 nm/min reported by Bumby [15] for bulk GaSb, as he has investigated deep (several micron) etching and notes that agitation is required to maintain fast etch rates: the observation indicates that the concentration of the active species drops quickly close to the semiconductor surface, leading to lower rates. On semiconductors containing antimony, a brown discolouration of the surface was frequently seen after etching; the film could be removed by dipping in concentrated HCl. Overall, the etch gave higher etch rates, better repeatability, and smoother surfaces than the tartrate etch and was therefore preferred for most mesa structures.

4.2.6 Reactive Ion Etching

Reactive ion etching (RIE), also referred to as dry etching, allows highly anisotropic etch rates and is therefore the preferred method for creating features with high aspect ratios, especially at the submicron scale. In a low-pressure, continuous-flow reaction chamber such as the one shown in Fig. 4.1(c), the process gases are exposed to a radio-frequency (RF) oscillating electric field above a planar electrode. The RF excitation ionizes the gases and forms a plasma containing radicals that can react with the sample placed on the electrode [1]; the chemical process itself may be isotropic or exhibit a degree of crystal-plane dependence. Anisotropy is a consequence of the large (typically several hundred volts) DC voltage that builds up because the DC-isolated electrode is charged by absorption of electrons from the plasma: transport of

Recipe	Freon 14 (sccm)	Argon (sccm)	Hydrogen (sccm)	Methane (sccm)	Power (W/cm^2)	Pressure (mTorr)
A			20·0	4·0	1·25	40·0
B		14·0	40·0	10·0	0·83	40·0
C			40·0	10·0	0·83	40·0
D	50·0				0·42	50·0

Table 4.1: RIE etch recipes

Recipe	GaSb (nm/min)	SiO_2 (nm/min)	Al (nm/min)	PMMA (nm/min)	ZEP (nm/min)	baked ZEP (nm/min)
A	$1·6 \pm 0·2$	$< 0·05$	$< 0·05$	> 30	> 30	
B	$1·7 \pm 0·2$	$< 0·05$	$< 0·05$	> 30		
C	$1·0 \pm 0·2$	$< 0·05$	$< 0·05$	20 to 30	20 to 30	4 to 10
D		16 ± 1		> 30	> 30	

Table 4.2: RIE etch rates

reactive ions depends on the electric field[1] corresponding to the potential difference and is highly directional. Dry etching of III–V semiconductors typically exhibits slow etch rates in comparison with silicon. While other chemistries have been explored, a hydrogen–methane plasma is often used as it gives good anisotropy and reproducibility for all III–V materials [5, 7,17]. SiO_2, which is used as an intermediate dielectric mask, can be etched readily in a freon-based plasma.

For these experiments, I used the OXFORD INSTRUMENTS RIE80+ plasma etcher depicted in Fig. 4.1(c). Table 4.1 lists the etch recipes employed in the present work. Recipe A followed the work of WERKING *et al.* [17], while recipe B had previously been used in Oxford by REHMAN [18]; recipe C was based on recipe B, but omitted the argon to achieve lower sputter rates on organic masks. Recipe D was a standard prescription for dry etching of silica.

Etch rates for the individual recipes are listed in Table 4.2. The etch rates for GaSb were quite low compared with published values [17]. In particular the rate for recipe B was approximately a third of that reported by REHMAN [18] on the same equipment. The reason

[1] Of the order 1 kV/m in conventional reaction chambers.

for this discrepancy is not fully understood. The etch rates listed here were determined by measuring step sizes after different process times with the help of a calibrated AFM and were corroborated for recipe C by the exposure of the InAs layer, which can be identified by its colour, after a suitable etch time. RIE in a continuous-flow reactor is quite sensitive to the process conditions. However, no significant increase in etch rate was obtained by varying power, pressure, and methane flow. The etch rates for organic resists could only be determined approximately, as their behaviour is non-linear: with the plasma formulae discussed here, initial etch rates were very high, but the resist was hardened with time. Presumably this was caused by a mechanism similar to the crosslinking that happens as a result of electron beam overexposure—exposed EBL resist that is not removed during development also was more resistant to the etch plasma. A further complication was the poor reproducibility of the thermal hardening of ZEP described in Sec. 4.2.2. Aluminium and silica did not etch appreciably in the hydrogen–methane plasmas used for structuring GaSb and InAs. However, peeling of the mask layers off the semiconductor surface was sometimes observed during long plasma exposures. Such peeling could be reduced, but not avoided completely, by careful cleaning of the surfaces before evaporation of the mask layer.

4.3 Transport Measurements

4.3.1 Magnets and Cryogenic Setup

Two superconducting magnets were used for most[2] magnetotransport measurements: an Oxford Instruments magnet with a maximal field of 18 T, which is shown in Fig. 4.9(a), and a state-of-the-art magnet, also manufactured by Oxford Instruments, with a maximal field of 21 T and a novel cryostat—see Fig. 4.9(b)—designed to reduce the helium evaporation rate. In both cases, the quoted field could only be obtained when the magnet was cooled to a temperature of 2·19 K. This temperature corresponds to the λ-point of ^{4}He and could be

[2] Some work was done on two other superconducting magnet systems very similar to the 18 T-magnet described here.

(a) Oxford Instruments 18 T superconducting magnet

(b) Oxford Instruments 21 T superconducting magnet

Figure 4.9: Magnets and cryogenic equipment

achieved in the volume below the lambda-plate without cooling down the entire ^{4}He bath. If used at the boiling point of ^{4}He, 4·23 K, which was often convenient for simplicity, the permissible fields were reduced to approximately 16 T and 19 T, respectively.

The sample under investigation could be immersed in the main bath either directly or within an insert filled with low pressure helium gas to facilitate heat exchange. For temperature dependent measurements, a variable temperature insert (VTI) was fitted to the 21 T-magnet, allowing the temperature to be controlled between 1·5 K and approximately room temperature; for the 18 T magnet, a ^{3}He-insert was available, allowing temperatures of 450 mK to be reached.

For both the VTI and the ^{3}He-refrigerator, sample holders including a rotation mechanism were available so that the sample could be turned about an axis perpendicular to the applied field from outside of the cryostat. The insert used with the VTI is shown in Fig. 4.10(a). Apart from making it possible to switch between perpendicular and parallel field configurations without having to take the sample out of the cryostat, such an arrangement facilitated studying the effect of an in-plane field on the magnetotransport. As illustrated in Fig. 4.10(b), in an external field $\mathbf{B}_0$ a sample rotated by an angle α from the parallel field configuration

(a) Rotating sample holder

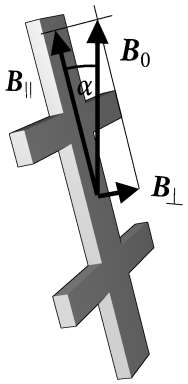

(b) Rotated Hall bar

Figure 4.10: Sample rotation

experiences a field $\mathbf{B}_\perp$ with magnitude $B_\perp = B_0 \sin\alpha$ in the normal direction and a field $\mathbf{B}_\parallel$ with magnitude $B_\parallel = B_0 \cos\alpha$ parallel to the surface. As long as α is small, the perpendicular field in the presence of a strong parallel field can be varied straightforwardly by rotating the sample, as $B_\perp \approx \alpha B_0$ and $B_\parallel \approx B_0$. For larger rotation angles these approximations do not hold: although rotation then does not provide a simple plot versus the smaller field component, the full parameter space in $B_\perp$ and $B_\parallel$ can still be mapped. An alternative approach, which was not attempted, would be to adjust B_0 to keep one of the components constant as the sample is rotated, *e.g.*, $B_0(\alpha) = B_\parallel / \cos\alpha$.

4.3.2 Electronic Measurements

The full two-dimensional conductivity tensor $\boldsymbol{\sigma}$ of a quasi-two-dimensional carrier system can be determined most straightforwardly in the Hall bar geometry shown in Fig. 4.11 [19]. Owing to the use of four-contact measurements, there is no contribution due to contact and lead resistances. The longitudinal resistivity is given by

$$\rho_{xx} = \frac{w}{\ell}\frac{V_{xx}}{I}, \tag{4.5}$$

while the Hall resistivity is calculated as

$$\rho_{xy} = \frac{V_{xy}}{I}. \tag{4.6}$$

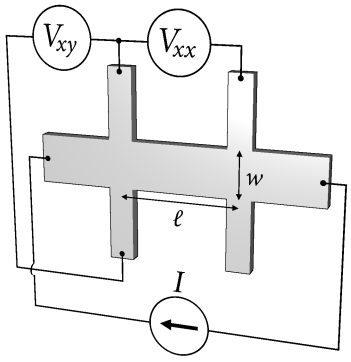

Figure 4.11: Measuring resistance in the Hall bar geometry

Assuming that $\rho_{yy} = \rho_{xx}$ and $\sigma_{yy} = \sigma_{xx}$,[3] the components of the conductivity tensor $\boldsymbol{\sigma} = \boldsymbol{\rho}^{-1}$ can be recovered from the well-known matrix relations

$$\sigma_{xx} = \frac{\rho_{xx}}{\rho_{xx}^2 + \rho_{xy}^2}; \qquad \sigma_{xy} = \frac{-\rho_{xy}}{\rho_{xx}^2 + \rho_{xy}^2}. \tag{4.7}$$

In practice, V_{xx} and V_{xy} were measured with a standard AC lock-in technique. The oscillator output of the lock-in amplifier was connected in series with a large adjustable resistor $R_{\text{series}} \gg R_{\text{sample}}$, where R_{sample} is the typical resistance between two contacts of the sample under investigation. If connected in an appropriate manner (*cf.* Fig. 4.11), the oscillator could thus act as a current source providing an excitation current $I \approx V_{\text{osc}}/R_{\text{series}}$. Because significant capacitive coupling between leads cannot be avoided in magnetotransport experiments, a low excitation frequency was desirable. Frequencies in the range 10 to 30 Hz were used, and care was taken to detune the reference frequency with respect to external sources of noise and circuit resonances. If a total of four lock-in amplifiers were used, V_{xx} and V_{xy} could be measured for two samples under identical experimental conditions as shown in Fig. 4.12. Alternatively, the voltages accross both pairs of contacts that a Hall bar provides for measuring each of ρ_{xx} and ρ_{xy} could be monitored simultaneously and compared for consistency. Measurements of this kind were routinely done over a limited field range after cooling down

[3] This assumption is reasonable for all samples discussed here, but will not hold true for anisotropic modulations.

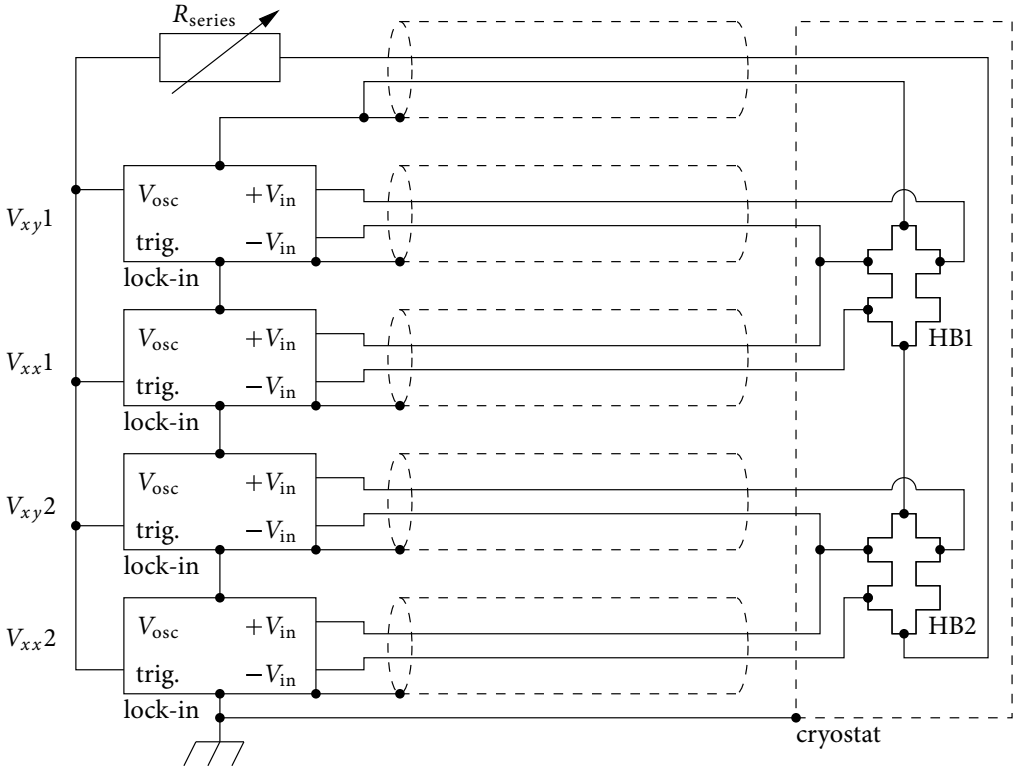

Figure 4.12: Set-up for measuring two samples with lock-in amplifiers

a sample and to investigate issues with individual samples (*cf.* Sec. 7.4.1), but most data were taken with a single pair of contacts for each Hall bar and independent resistivity component.

4.3.3 Fabrication of Hall bars

Hall bars for such measurements were produced by defining a suitably shaped mask on top of a DHET by optical lithography. The process is illustrated in Fig. 4.13: After lithography, wet chemical etching was used to create a Hall-bar-shaped mesa between 0·5 and 1·0 µm high. As the InAs layers lay between 50 and 150 nm below the surface, the quasi-two-dimensional electron and hole gases were confined to the shape of the mesa, which contained areas forming broad contact leads and contact pads as shown in Fig. 4.14. A second photoresist mask was then created on top of the mesa, which left holes at the contact pads. In an evaporator the sample was covered with a metallization consisting of 8 nm nickel, 140 nm eutectic

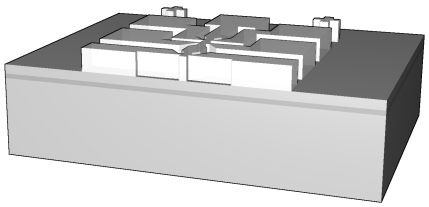

(a) Definition of Hall bar mask

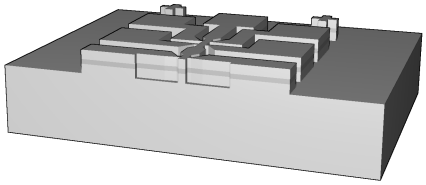

(b) Pattern transfer

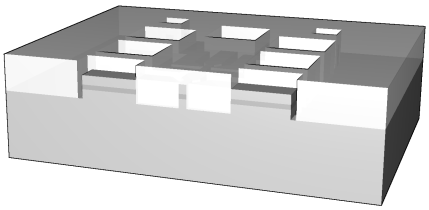

(c) Definition of contact mask

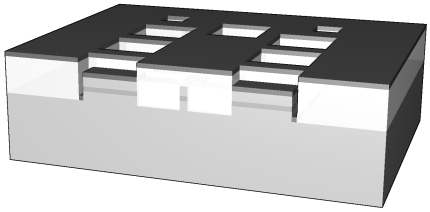

(d) Evaporation of contact metallization

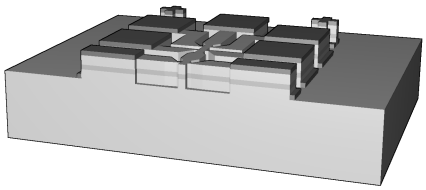

(e) Lift-off

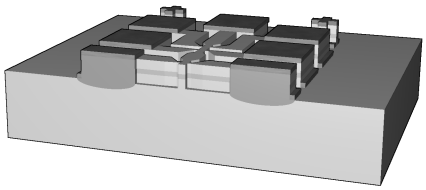

(f) Annealing

Figure 4.13: Fabrication of Hall bars for transport measurements. The vertical scale is exaggerated.

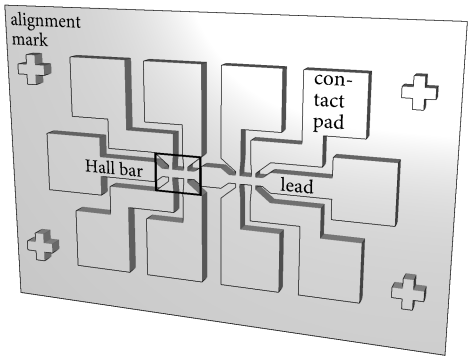

Figure 4.14: Hall bar mesa

gold–germanium alloy, a further 60 nm nickel, and finally 150 to 300 nm of gold. The nickel layers served to improve adhesion. In the next step, the metallization was lifted off the mesa except for the contact pads by dissolving the photoresist in acetone or resist stripper. Thin gold layers were preferred as they made lift-off easier. Finally, the contact metallization was annealed for 30 s at 390 °C. During this process, germanium diffused into the GaSb cap layer, forming an ohmic contact between the InAs quantum well and the remaining contact metal. The sample could then be attached to a suitable package, and the contact pads could be connected with a wire bonder. I used a Kulicke & Soffa 4124 manual gold ball bonder for this purpose.

4.4 Summary

As will be explained in Chapter 5, quasi-two-dimensional carrier systems appear at InAs–GaSb heterointerfaces. Magnetotransport measurements of a small portion of the carrier sheets that form in thin epitaxial heterostructures can be performed by patterning the surface layer of a suitable sample in the form of a conventional Hall bar. This is readily done using a combination of standard optical lithography and wet chemical etching techniques; details of their implementation in relation to the present work have been given. The resolution of these methods is sufficient to create Hall bars with sizes down to 5 µm × 15 µm. I have outlined how

such devices can be used to measure the resistivity (and hence conductivity) of the carriers at low temperatures as a function of external magnetic fields parallel or perpendicular to the plane of the surface.

Imposing a lateral modulation on the Hall bars that has a period much smaller than the mean free path in the carrier systems requires technologies capable of much higher resolution. One such technology is standard electron beam lithography (EBL). Access to expensive state-of-the-art equipment is, however, required to achieve sufficient resolution; this is particularly true as dense antidot patterns are especially susceptible to proximity effects caused by secondary electrons. Another problem with EBL is the incompatibility of the commonly used resist materials with deep reactive ion etching (RIE) of III–V semiconductors. Yet RIE, as a highly anisotropic etch technique, is required for the creation of pits with high aspect ratios. The difficulty can be circumvented by introducing an intermediate dielectric mask that stands up well to the etch plasma.

I have developed alternative lithographic techniques based on atomic force microscopy (AFM). Local anodic oxidation (LAO), described in Chapter 3, can be used to remove designated areas of the semiconductor surface with high resolution. However, the etch depth attainable with this technique is fundamentally limited and has ultimately proven insufficient for imposing a lateral modulation on the structures investigated in the present work. Special consideration has therefore been given to the possibility of using LAO to fabricate RIE etch masks. The chemical incompatibilities involved in the creation of a thin aluminium mask on GaSb can be avoided by introducing a silica spacer layer to isolate the mask from the antimonide.

Bibliography

[1] M. J. Kelly. *Low-Dimensional Semiconductors*, chapter 3. Series on semiconductor science and technology. Oxford University Press, Oxford, England, 1995.

[2] D. R. Medeiros, A. Aviram, C. R. Guarnieri, W.-S. Huang, R. Kwong, C. K. Magg, A. P. Mahorowala, W. M. Moreau, K. E. Petrillo, and M. Angelopoulos. Recent progress in

electron-beam resists for advanced mask-making. *IBM Journal of Research and Development*, 45(5):639–650, 2001.

[3] A. C. F. Hoole, M. E. Welland, and A. N. Broers. Negative PMMA as a high-resolution resist—the limits and possibilities. *Semiconductor Science and Technology*, 12:1166–1170, 1997.

[4] W. Chen and H. Ahmed. Fabrication of sub-10 nm structures by lift-off and by etching after electron beam exposure of poly(methylmethacrylate) resist on solid substrates. *Journal of Vacuum Science and Technology B*, 11(6):2519–2523, November/December 1993.

[5] J. R. Lothian, F. Ren, and S. J. Pearton. Mask erosion during dry etching of deep features in III–V semiconductor structures. *Semiconductor Science and Technology*, 7(9):1199–1209, 1992.

[6] R. M. Nyffenegger and R. M. Penner. Nanometer-scale surface modification using the scanning probe microscope: Progress since 1991. *Chemical Reviews*, 97:1195–1230, 1997.

[7] B. Schmidt, S. Illek, B. Borchert, J. Rieger, and M.-C. Amann. Tunable twin guide laser diodes with high output efficiency fabricated by an improved reactive ion etching technique. *Semiconductor Science and Technology*, 13:821–825, 1998.

[8] K. R. Williams, K. Gupta, and M. Wasilik. Etch rates for micromachining processing—part II. *Journal of Microeletromechanical Systems*, 12(6):761–778, December 2003.

[9] P. M. Campbell, E. S. Snow, and P. J. McMarr. AFM-based fabrication of Si nanostructures. *Physica B*, 227:315–317, 1996.

[10] P. A. Fontaine, E. Dubois, and D. Stiévenard. Characterization of scanning tunneling microscopy and atomic force microscopy-based techniques for nanolithography on hydrogen-passivated silicon. *Journal of Applied Physics*, 84(4):1776–1781, August 1998.

[11] A. Boisen, K. Birkelund, O. Hansen, and F. Grey. Fabrication of submicron suspended structures by laser and atomic force microscopy lithography on aluminum combined with reactive ion etching. *Journal of Vacuum Science and Technology B*, 16(6):2977–2981, November/December 1998.

[12] G. Abadal, A. Boisen, Z. J. Davis, O. Hansen, and F. Grey. Combined laser and atomic force microscope lithography on aluminum: Mask fabrication for nanoelectromechanical systems. *Applied Physics Letters*, 74(21):3206–3208, 1999.

[13] A. Boisen. Private communication, 2004.

[14] J. G. Buglass, T. D. McLean, and D. G. Parker. A controllable etchant for fabrication of GaSb devices. *Journal of The Electrochemical Society*, 133(12):2565–2567, December 1986.

[15] C. W. Bumby. *Thermophotovoltaic Devices based upon Heteroepitaxial GaSb grown by MOVPE*. DPhil thesis, Hertford College, University of Oxford, 2005.

[16] S. Adachi, H. Kawaguchi, and G. Iwane. A new etchant system, $K_2Cr_2O_7$–H_2SO_4–HCl, for GaAs and InP. *Journal of Materials Science*, 16(9):2449–2456, 1981.

[17] J. Werking, J. Schramm, C. Nguyen, E. Hu, and H. Kroemer. Methane/hydrogen-based reactive ion etching of InAs, InP, GaAs, and GaSb. *Applied Physics Letters*, 58(18):2003–2005, May 1991.

[18] Y. J. Rehman. *Processing and Magneto-transport Studies of InAs/GaSb Low Dimensional Structures*. DPhil thesis, The Queen's College, University of Oxford, 1999.

[19] C. Weisbuch and B. Vintner. *Quantum Semiconductor Structures*, chapter IV. Academic Press, San Diego, California, 1991.